Compact, Hybrid III-V/Silicon Vernier Laser Diode Operating From 1955–1992 nm

Jia Xu Brian Sia, Xiang Li, Wanjun Wang, Zhongliang Qiao, X. Guo, Jiawei Wang, Callum G. Littlejohns, Chongyang Liu, Graham T. Reed, Kian Siong Ang, and Hong Wang

***Abstract*—The 2 μm waveband is capable of enabling pervasive applications. The demonstration of the hollow-core photonic bandgap fiber and the thulium-doped fiber amplifier has highlighted the fiber propagation and amplification aspects of fiber communications, indicating its potential as an adjunct to present communication infrastructure at the O/C bands. The above is especially imperative given the current concerns with regards to the upper bandwidth limit of the single-mode fiber. Furthermore, the waveband could facilitate many more applications such as LIDAR and free-space communication. However, water absorption (OH^-) is high at most of the 2 μm waveband and this will impact the optical insertion loss of applications implemented in the wavelength region. The relative low water absorption region of the waveband falls within 1950 – 2000 nm. As such, the development of a hybrid/heterogeneous III-V/silicon laser source that operates within the region is important for 2 μm silicon photonics. In this work, we demonstrate a III-V/Si hybrid tunable laser operating from 1955 - 1992 nm for the first time. Room temperature continuous wave operation is achieved with a maximum laser output power of 8.1 mW. This wavelength-tunable laser operates specifically within the low water absorption window, indicating good wavelength suitability for applications at the 2 μm waveband.**

***Index Terms*—2 μm silicon photonics, hybrid III-V/silicon lasers, integrated optics, tunable lasers.**

I. Introduction

THE primary advantage of wavelength-tunable lasers lies in its ability to reduce the complexity of optical systems; a single wavelength-tunable laser can be used to replace an array of single-wavelength lasers, thereby, simplifying system architectures as well as lowering inventory costs. The crux in the realization of such lasers, depends on the integration of a wavelength-selective mechanism and an optical gain-section. While distributed feedback (DFB) laser arrays and microelectromechanical systems (MEMS) vertical cavity surface emitting lasers (VCSEL) has been shown to demonstrate wavelength-tuning functionality, there may be limitations in terms of DFB array coupler loss [1] and mechanical instability [2] respectively. Littman/Littrow-configured external cavity lasers (ECL) have also indicated wide spectral operating range, but however, the application-space of these class of lasers are limited by their bulk [3], as well as higher vulnerability to environmental vibrations [4]. The challenge is for the development of a solid state-based laser diode with a compact footprint, good performance (i.e., tuning range, output power) that can be manufactured in a scalable, high-yield and low-cost process. Silicon photonic platform, backed by the economies of trillions of dollars of investment into silicon manufacturing poses an attractive proposition for the realization of the abovementioned laser diode. However, due to the indirect bandgap of silicon and germanium, the realization of an electrically-pumped group IV laser remains elusive. Hybrid/heterogenous silicon photonics, integrating silicon photonic passives and III-V gain medium offers the best of both worlds [5]–[8]. Silicon photonics enables low propagation loss, high integration densities while III-V materials enables efficient optical gain and flexibility for spectral-engineering.

The high-index contrast of the silicon-on-insulator (SOI) platform enables low-loss microrings (MRRs) to be designed with tight bending radius. As a result, Vernier filters with a large free-spectral range (FSR) can be achieved [9]. To date, extensive work has been reported in Vernier-based silicon photonic diode lasers operating near the C-band [9]–[13]. Instances, while not limited to, include enhanced spectral range [9], power [10] and side-mode suppression ratio (SMSR) [11], [13].

Recent trend in silicon photonics suggests an extension from the traditional wavebands of O and C to exploit potential applications [14]–[21]. Much interest has been geared towards the 2 μm waveband specifically due to numerous applications it entails [14]–[21]. The 2 μm waveband is a plausible "window" for fiber communications in view of the favorable performance of the hollow core-photonic bandgap fiber (HC-PBGF) [22]–[23] and thulium-doped fiber amplifier (TDFA) [24]–[25]. Applications beyond fiber communications, while not exhaustive includes

Manuscript received June 21, 2021; revised September 25, 2021; accepted October 10, 2021. Date of publication October 14, 2021; date of current version November 9, 2021. This work was supported in part by the National Research Foundation of Singapore NRFCRP12-2013-04 and RIE2020 IAF-ICP under Grant 12001E0060 and in part by NTU-CompoundTek Research Collaboration Agreement RCA #020263-00001. *(Corresponding author: Hong Wang.)*

Jia Xu Brian Sia is with the School of Electrical and Electronic Engineering, Nanyang Technological University, Singapore 639798, Singapore, and also with the CompoundTek, 5 International Business Park, Singapore 609914, Singapore (e-mail: jiaxubri001@e.ntu.edu.sg).

Xiang Li and Chongyang Liu are with the Temasek Laboratories@NTU(TL@NTU), Nanyang Technological University, Singapore 637553, Singapore (e-mail: x.li@ntu.edu.sg; liucy@ntu.edu.sg).

Wanjun Wang, Zhongliang Qiao, X. Guo, Jiawei Wang, and Hong Wang are with the School of Electrical and Electronic Engineering, Nanyang Technological University, Singapore 639798, Singapore (e-mail: wangwanjun1010@hotmail.com; qzhl2007@hotmail.com; tguoxin@ntu.edu.sg; jiawei010@e.ntu.edu.sg; ewanghong@ntu.edu.sg).

Callum G. Littlejohns and Graham T. Reed are with the Optoelectronics Research Centre, University of Southampton, SO17 1BJ Southampton, U.K. (e-mail: c.littlejohns@soton.ac.uk; g.reed@soton.ac.uk).

Kian Siong Ang is with the CompoundTek, 5 International Business Park, Singapore 609914, Singapore (e-mail: ksang@compoundtek.com).

Digital Object Identifier 10.1109/JPHOT.2021.3119760

LIDAR [26], free-space communications [27], optical logic and signal processing [17]. However, it is important to note that water is strongly-absorbing at most of the 2 μm waveband; this will lead to increased optical insertion loss in applications at the waveband. The relative low water absorption region falls within 1950 – 2000 nm [28], thereby, it is important to realize laser sources on the silicon photonics platform that operates within the wavelength region.

Crucial to the development of silicon photonics-based coherent, tunable light sources that can unlock the aforementioned applications, involves the design of silicon photonics-based wavelength-selective cavity and III-V optical amplifier. Thus far, there are two pathways towards the realization of electrically-pumped spectral emission near 2 μm; InP-based type-II active region and GaSb-based type-I active region structures [29]–[30]. However, the GaSb-based platform appears to demonstrate better performance due to the need to apply larger strain on the quantum wells in the InP-based platform, thus, potentially giving rise to higher defect-density, impacting performance [30].

In this work, we report a silicon hybrid ring external cavity (SHREC)/ InGaSb-AlGaAsSb wavelength-tunable laser diode operating from 1955-1992 nm for the first time; minimum side-mode suppression ratio (SMSR) of 25 dB is characterized. As mentioned earlier, the wavelength-tunable laser operates specifically within the relative low water-absorption region of the 2 μm waveband. The maximum measured laser output power is 8.1 mW under room-temperature continuous wave operation (RT-CW) condition.

II. Hybrid III-V/Silicon Vernier Laser Diode

The 3-D schematic of the wavelength-tunable laser diode is illustrated in Fig. 1(a); the micrograph images of the device is shown in Fig. 1(b). The hybrid laser is composed by edge-coupling the wavelength-tunable Vernier cavity to the SOA via the Si slab waveguide (6×0.07 μm^2) and spot-size converter (SSC). Lasing output occurs at the facet as indicated (Fig. 1(a)). The Si slab waveguide enables mode matching with the SOA and the SSC facilitates subsequent transition to the wavelength selective Vernier cavity. The coupling loss between the SOA and the wavelength-tunable Vernier cavity is experimentally characterized to be 2.7 dB; the coupling loss comprises of the optical loss from the SOA to the silicon slab waveguide, then the SSC in which a testing structure is used. The SOA provides optical gain. Wavelength selective feedback is enabled by the Vernier effect of the 2 MRRs in the Vernier cavity; the radii (R) of the two MRRs are 16.8 (mrr1) and 18.2 (mrr2) μm. The gap between the MRRs and the bus waveguide is 180 nm. Based on our prior work investigating the effect of gap between the MRRs and the bus waveguide on laser performance, it is found that 180 nm enables relatively higher slope efficiency, laser output power and lower threshold current (I_{th}) [19]. We would like to emphasize, however, that the gap selection is not optimal for SMSR [19].

The resonance of the individual MRRs (T_{mrr1}, T_{mrr2}) as computed in Fig. 2 when zero power is applied to either of the phase shifters ($H_{mrr1} = H_{mrr2} = 0$ mW), can be thermo-optically

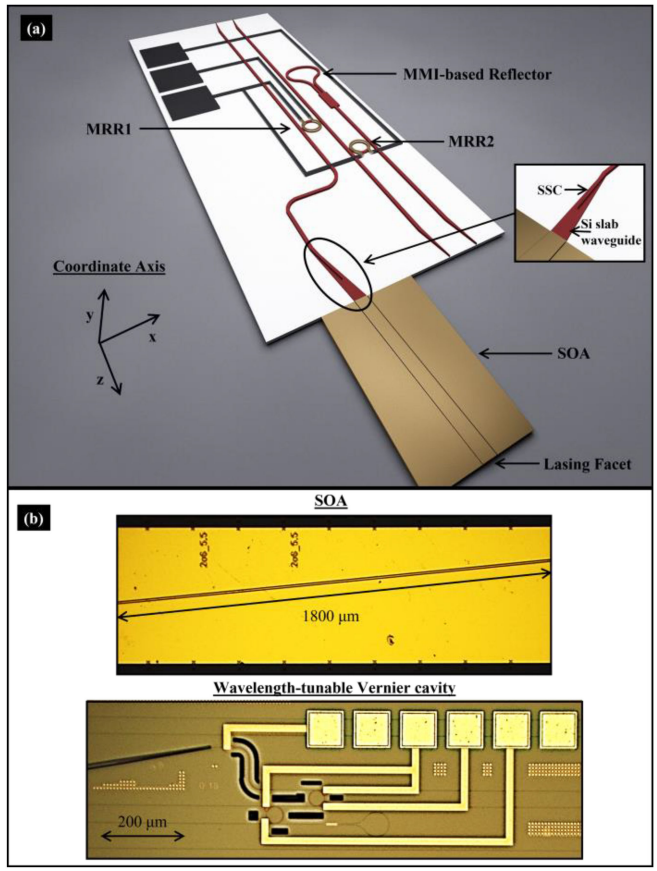

Fig. 1. (a) 3-D schematic of the wavelength-tunable laser diode; coordinate axis is indicated. (b) Micrograph images: SOA at the top, wavelength-tunable Vernier cavity at the bottom.

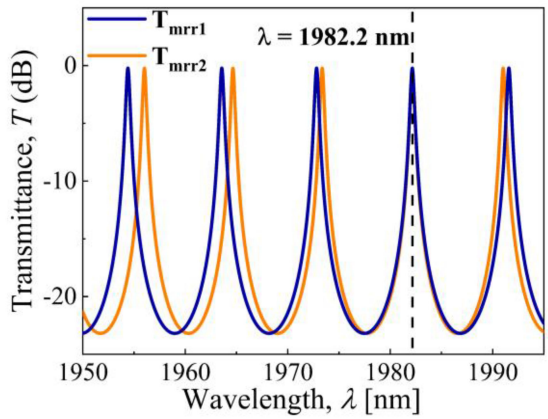

Fig. 2. Theoretical individual transmittance spectra of 2 MRRs (T_{mrr1}, T_{mrr2}). When no power is applied to the 2 phase shifters ($H_{mrr1} = H_{mrr2} = 0$ mW), the 2 resonances will overlap at 1982.2 nm.

controlled through the phase-shifters mounted on top of the two MRRs. The laser cavity will experience least loss at the wavelength where the two MRRs overlaps and lase via mode competition. Thereby, wavelength-tuning functionality of the laser diode can be achieved; in the operating condition of Fig. 2,

the resonance of the two MRRs are theoretically predicted by (1) as shown at the bottom of the page, to overlap at 1982.2 nm. The θ is the accumulated phase of the lightwave after propagating one round in the MRR, κ is the electric field coupling coefficient and α corresponds to the loss coefficient of the waveguide. The operating principle of the Vernier cavity will be further elaborated theoretically and experimentally in the following section.

The wavelength-selective Vernier cavity is fabricated on the 220 nm SOI platform via the CMOS the standard CMOS process line. The propagation loss of the strip waveguide, with dimensions of 0.6 × 0.22 μm^2 and Q-factor of the MRRs are experimentally characterized to be 3 dB/cm and 4921 respectively. Proceeding the fabrication of the waveguides, 1.2 μm of SiO_2 cladding is deposited followed by 2 μm of Al for routing and 0.12 μm of TiN for the heaters.

III. Wavelength-Selective Vernier Cavity

The wavelength selective Vernier cavity consists of a 1 × 2 MMI-based reflector and a Vernier filter; designed for the fundamental TE mode. The MMI is optimized at $\lambda \approx 1970$ nm, the central wavelength of the amplified spontaneous emission (ASE) from the SOA. The width and the length of the MMI coupler is 6 and 22.7 μm respectively. The output tapers of the MMI coupler, 20 μm-long, tapers from 135 μm to 0.6 μm. The tapers on the two output end of the MMI coupler are spaced apart by 3.14 μm. With FSRs of 9.2 (mrr1) and 8.7 nm (mrr2), the FSR of the Vernier filter is 140 nm, as determined by (2).

The theoretical Vernier transmittance spectra ($T_{theo.}$), as shown in Fig. 3(a)-(b), can be computed as a product of the individual transmittances of the MRRs (Fig. 2). Due to the limited spectral range of our light source, the Vernier filter was characterized from $\lambda = 1950 – 1995$ nm ($T_{exp.}$). Fig. 3(a)-(b) indicates close correspondence between $T_{theo.}$ and $T_{exp.}$; the noise floor of the detector is below 21 dB (shaded), as such, measurement lower than that is not possible. As predicted by Fig. 2, the wavelength corresponding to the Vernier transmittance peak when $H_{mrr1} = H_{mrr2} = 0$ mW is measured to be $\lambda = 1982.2$ nm. When $H_{mrr1} = 2.94$ mW, $H_{mrr2} = 0$ mW, the resonant peak of mrr1 would red-shift by 0.54 nm and overlap with the resonance of mrr2 at $\lambda = 1973.34$ nm, resulting in a Vernier peak with a measured modal transmittance difference ($MTD_{exp.}$) of 5.89 dB. The insertion loss of the Vernier peak is 1.9 dB (Fig. 3(b).

$$FSR\,(Vernier) = \left| \frac{FSR\,(r = 16.8\ \mu m) \times FSR\,(r = 18.2\ \mu m)}{FSR\,(r = 16.8\ \mu m) - FSR\,(r = 18.2\ \mu m)} \right| \quad (2)$$

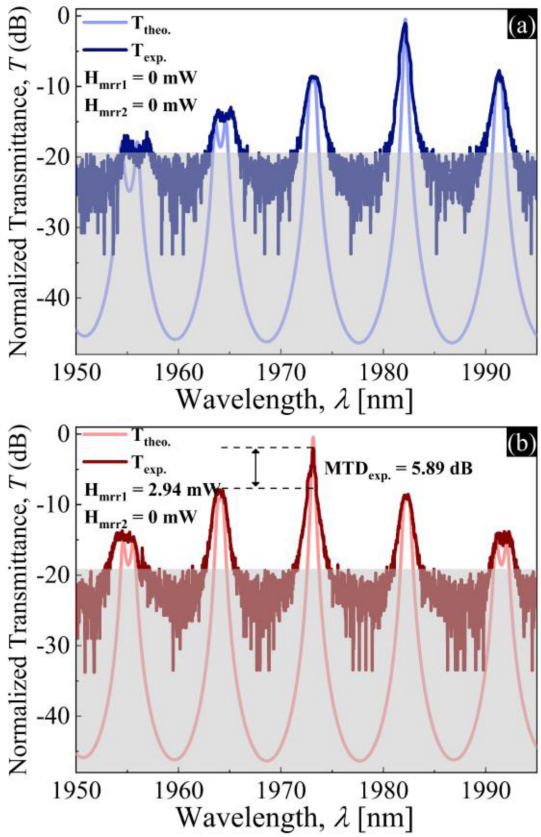

Fig. 3. Theoretical and experimental Vernier Transmittance spectra when (a) Hmrr1 = Hmrr2 = 0 mW, (b) Hmrr1 = 2.94 mW, Hmrr2 = 0 mW.

IV. GaSb-Based SOA

The designed epitaxial structure of the SOA, grown on a (100) n-GaSb substrate through molecular beam epitaxy (MBE) is illustrated in Fig. 4(a). 1.26% of compressive strain is applied to 10 nm-think $In_{0.2}Ga_{0.8}Sb$ single quantum well which is sandwiched between 270 nm-thick $Al_{0.5}GaAsSb$ barriers.

The barrier and cladding layers are lattice-matched to the GaSb substrate. Detailed fabrication steps are elaborated in our previous work [31]. After the fabrication, the SOA is bonded to a heat sink for efficient temperature control. The cross-sectional dimensional of the SOA ridge waveguide is 5.7 × 1.2 μm^2. In Fig. 4(b), the spontaneous emission spectra, coupled via a lensed fiber to the optical spectrum analyzer (OSA) corresponding to bias current (I_{bias}) levels of 100, 200, 300, 400, 500 mA is presented; a clear emission window from 1.8 to 2.1 μm is measured. As the current is increased, there is only a slight redshift of the spontaneous emission spectra which can be attributed to effective thermal control of the SOA. The SOA waveguide tilted at 5 degrees, is shown to successfully suppress Fabry-Perot oscillations; Fig. 4(b) resembles the spontaneous emission spectra measured from our previous work [32].

$$P_{ring1,2} = \left| \frac{-\kappa^* \kappa \sqrt{\alpha} \exp(j\sqrt{\theta(\mathrm{R} = 16.8, 18.2\mu\mathrm{m})}}{1 - (\sqrt{1 - |\kappa^2|})^* (\sqrt{1 - |\kappa^2|})^* \alpha \exp(j\theta(\mathrm{R} = 16.8, 18.2\mu\mathrm{m})} \right|^2 \quad (1)$$

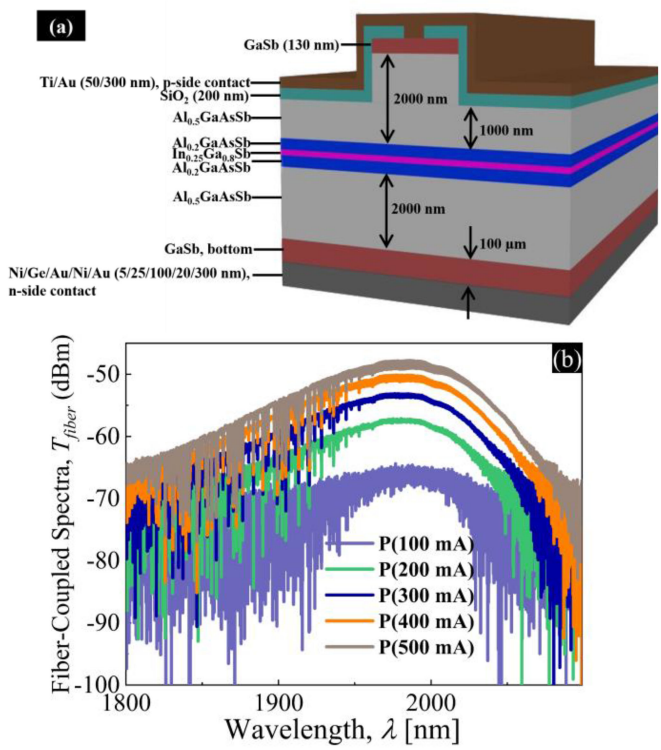

Fig. 4. (a) Designed epitaxial structure of GaSb-based SOA, (b) measured spontaneous emission spectra of GaSb-based SOA at I_{bias} = 100, 200, 300, 400, 500 mA.

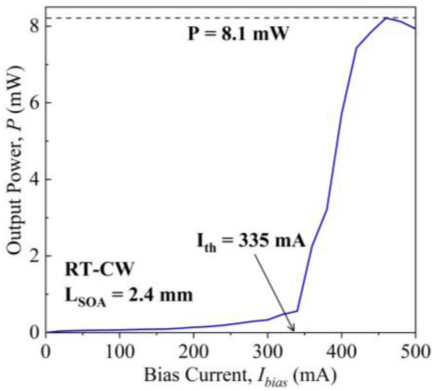

Fig. 5. L-I of the wavelength-tunable laser diode.

V. Laser Characterization

The SOA is hybrid integrated to the silicon photonic chip via the active alignment approach. The near-field mode field diameter of the silicon slab waveguide and SOA are 5.5 × 0.9 μm^2 and 5.5 × 1.0 μm^2 respectively. Analysis in regard to the alignment tolerances between the SOA and silicon photonic chip during active alignment is presented in our previous work [18]; the coordinate axis is indicated in Fig. 1(a). The y-axis indicates low alignment tolerance, where a 0.5 μm misalignment leads to a 6 dB coupling loss. The x and z-axis have larger coupling tolerance, where a 0.5 μm misalignment leads to 1.58 and 1.79 dB coupling loss respectively. The L-I of the laser, as shown in Fig. 5, under RT-CW condition,

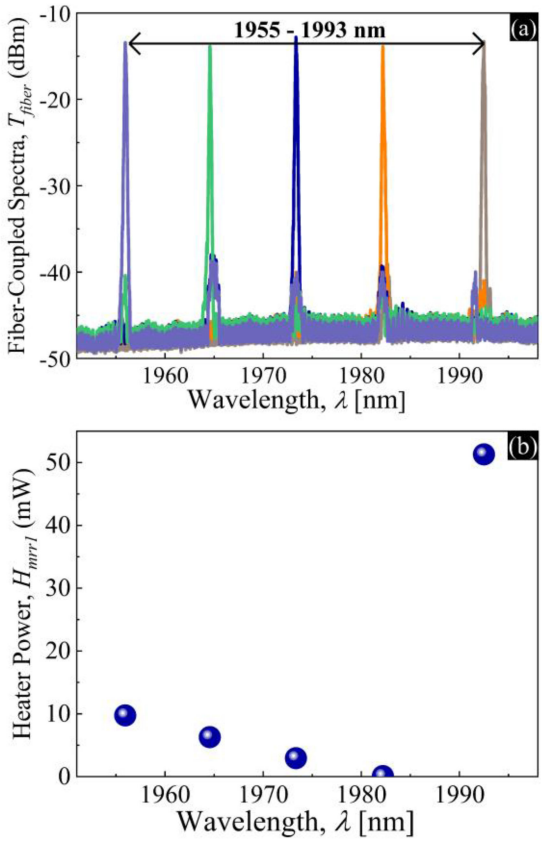

Fig. 6. (a) Superimposed lasing spectra (I_{bias} = 420 mA), (b) corresponding heater power for each demonstrated lasing wavelength.

was obtained by directly coupling the laser emission into the aperture of the power-detector. An I_{th} of 335 mA was obtained; the threshold current could be attributed to the significant hybrid integration coupling loss between the SOA and the wavelength-tunable Vernier cavity as abovementioned (2.7 dB). The maximum demonstrated on-chip output power is 8.1 mW.

In a similar fashion to the characterization of Fig. 4(b), the tuning range of the wavelength-tunable laser diode was measured by coupling the laser emission to the OSA through a lensed-fiber. Fig. 6(a) illustrates the superimposed discrete lasing spectra from 1955-1992 nm, obtained when H_{mrr1} is tuned with a minimum SMSR of 25 dB; heater values corresponding to each wavelength is indicated in Fig. 6(b). I_{bias} is 420 mA. As abovementioned, the selection of the coupling gap between the MRRs and the bus waveguide is for relatively higher laser slope efficiency, output power and lower I_{th}. The coupling gap does not correspond to the optimal value for SMSR. This is due to the relatively lower MTD of the vernier filter and thereby, reduced wavelength selectivity of the laser cavity. Further improvement of the SMSR can be enabled by increasing the wavelength selectivity of the laser cavity through an increase in the coupling gap between the MRRs and the bus waveguide [19] or the addition of more wavelength filtering components; a wavelength-tunable Mach-Zehnder interferometer [12] or the further addition of MRRs [13]. Fig. 6(a) indicates the maximum tuning range of the laser. As mentioned earlier, by exploiting the Vernier effect,

the wavelength-dependent hybrid cavity loss can be controlled, leading to wavelength-selective lasing via mode competition. In Fig. 6(a), as H_{mrr1} is tuned (Fig. 6(b)), the resonance of mrr1 will redshift and overlap consecutively at the resonant wavelengths of mrr2 (Fig. 2); Vernier peak will be formed at the resonant wavelengths of mrr2 as H_{mrr1} is increased. As it can be seen, the spacing between the superimposed lasing peaks correspond to the FSR of mrr2 (Fig. 6(a)). While Fig. 6(a) illustrates discrete tuning, one can simply realize fine tuning through the thermo-optic control of both H_{mrr1} and H_{mrr2}. Fine tuning down to resolution of 0.5 nm has been demonstrated in our prior work [18], [20]. For the first three lasing wavelengths from the left of Fig. 6(a), it can be seen that the heater power required to lase at the specific wavelength reduces from the left. This can be explained by Fig. 2, as the distance between the mrr1 and mrr2 resonance reduces from the left for the first three sets of resonances. As indicated in Fig. 6(b), for the fourth lasing wavelength from the left of Fig. 6(a), the heater power is 0 mW. This is due to the fourth set of resonance from the left in Fig. 2 overlapping. For the first lasing wavelength from the right in Fig. 6(a), there is a huge jump in heater power as indicated in Fig. 6(b) as the fourth mrr1 resonance from the left would have to redshift about one FSR of mrr2 to overlap with the first mrr2 resonance from the right. For the laser operation demonstrated within this work, no mode-hopping is observed. However, mode hopping is to be expected and can be overcome using active longitudinal mode optimization through the thermo-optic effect.

VI. Conclusion

The 2 μm waveband, is an attractive proposition in view of its wide range of applications. This has stimulated an uptake in the development of silicon photonic devices operating at the waveband. However, most of the 2 μm waveband is subject to strong water absorption, which will impact applications at the wavelength region. In this work, we report the development of III-V/Si hybrid tunable lasers operating from 1955-1992 nm, which corresponds to the relative low water absorption region of the 2 μm waveband. RT-CW operation is achieved with a maximum output power of 8.1 mW.

References

[1] B. Mroziewicz, "External cavity wavelength tunable semiconductor lasers-a review," *Opto-Electron. Rev.*, vol. 16, no. 4, pp. 347–366, 2008.

[2] S. J. Park, G. H. Kim, H. D. Lee, C.-S. Kim, and M. Jo, "Narrowing linewidth of wavelength-swept active mode locking laser based on cross gain modulation," *Appl. Sci.*, vol. 9, no. 19, 2019, Art. no. 4029.

[3] R. Wang, "III-V/silicon photonic integrated circuits for spectroscopic sensing in the 2-2.5 μm wavelength range," Ph.D. dissertation, Dept. of Signal Processing and Acoustics, Gent Univ., 2018.

[4] T. Hieta, "Applied diode laser spectroscopy and characterization of optical fiber nonlinearity," Ph.D. dissertation, Dept. of Signal Processing and Acoustics, Aalto Univ., 2011.

[5] T. Komljenovic *et al.*, "Heterogenous silicon photonic integrated circuits," *J. Lightw. Technol.*, vol. 34, no. 1, pp. 20–35, 2016.

[6] M. A. Tran, D. Huang, and J. E. Bowers, "Tutorial on narrow linewidth tunable semiconductor lasers using Si/III-V heterogenous integration," *APL Photon.*, vol. 4, 2019, Art. no. 111101.

[7] C. O. de Beeck *et al.*, "Heterogenous III-V on silicon nitride amplifiers and lasers via microtransfer printing," *Optica*, vol. 7, no. 5, pp. 386–393, 2020.

[8] T. Kita, N. Yamamoto, T. Kawanishi, and H. Yamada, "Ultra-compact wavelength-tunable quantum-dot laser with silicon photonics double ring filter," *Appl. Phys. Exp.*, vol. 8, 2019, Art. no. 062701.

[9] K. Boller *et al.*, "Hybrid integrated semiconductor lasers with silicon nitride feedback circuits," *Photonics*, vol. 7, no. 4, 2020.

[10] N. Kobayashi *et al.*, "Silicon photonic hybrid ring-filter external cavity wavelength tunable lasers," *J. Lightw. Technol.*, vol. 33, no. 6, pp. 1241–1246, 2015.

[11] H. Guan *et al.*, "Widely-tunable, narrow-linewidth III-V/silicon hybrid external-cavity laser for coherent communication," *Opt. Exp.*, vol. 26, no. 7, pp. 7920–7933, 2018.

[12] T. Kita, R. Tang, and H. Yamada, "Compact silicon photonic wavelength-tunable laser diode with ultra-wide wavelength tuning range," *Appl. Phys. Lett.*, vol. 106, 2015, Art. no. 11104.

[13] Y. Fan *et al.*, "Hybrid integrated InP-Si_3N_4 diode laser with a 40-Hz intrinsic linewidth," *Opt. Exp.*, vol. 28, no. 16, pp. 21713–21728, 2020.

[14] Y. Yin *et al.*, "High-speed and high-responsivity hybrid silicon/black-phosphorus waveguide photodetectors at 2 μm," *Laser Photon. Rev.*, vol. 13, 2019, Art. no. 1900032.

[15] X. Li *et al.*, "30 GHz GeSn photodetector on SOI substrate for 2 μm wavelength application," *Photon. Res.*, vol. 9, no. 4, pp. 494–500, 2021.

[16] W. Cao *et al.*, "High-speed silicon modulators for the 2 μm band," *Optica*, vol. 5, no. 9, pp. 1055–1062, 2018.

[17] F. Gunning and B. Corbett, "Time to open the 2-μm window?," *Opt. Photon. News*, vol. 30, no. 3, pp. 42–47, 2019.

[18] J. X. B. Sia *et al.*, "Compact silicon photonic hybrid ring external cavity (SHREC)/InGaSb-AlGaAsSb wavelength-tunable laser diode operating from 1881-1947 nm," *Opt. Exp.*, vol. 28, no. 4, pp. 5134–5146, 2020.

[19] J. X. B. Sia *et al.*, "Analysis of compact silicon photonic hybrid ring external cavity (SHREC) wavelength-tunable laser operating from 1881-1947 nm," *IEEE J. Quantum Electron.*, vol. 56 no. 6, 2020, Art. no. 20011311.

[20] J. X. B. Sia *et al.*, "Sub-kHz linewidth, hybrid III-V/silicon wavelength-tunable laser diode operating at the application rich 1647–1690 nm," *Opt. Exp.*, vol. 28, no. 17, pp. 25215–25224, 2020.

[21] R. Wang, A. Malik, I. Šimonyte, A. Vizbaras, K. Vizbaras, and G. Roelkens, "Compact GaSb/silicon-on-insulator 2.0x μm widely tunable external cavity lasers," *Opt. Exp.*, vol. 24, no. 25, pp. 28977–28986, 2016.

[22] P. J. Roberts *et al.*, "Ultimate low loss of hollow-core photonic crystal fibres," *Opt. Exp.*, vol. 13, no. 1, pp. 236–244, 2005.

[23] B. J. Mangan *et al.*, "Low loss (1.7 dB/km) hollow core photonic bandgap fiber," in *Proc. Opt. Fiber Commun. Conf.*, 2004.

[24] Z. Li, A. M. Heidt, J. M. O. Daniel, Y. Jung, S. U. Alam, and D. J. Richardson, "Thulium-doped fiber amplifier for optical communications at 2 μm," *Opt. Exp.*, vol. 21, no. 8, pp. 9289–9297, 2013.

[25] Z. Li *et al.*, "Diode-pumped wideband thulium-doped fiber amplifiers for optical communications in the 1800–2050 nm window," *Opt. Exp.*, vol. 21, no. 22, pp. 26450–26455, 2013.

[26] T. M. Taczak and D. K. Killinger, "Development of a tunable, narrow-linewidth, cw 2066-μm Ho:YLF laser for remote sensing of atmospheric CO_2 and H_2O," *Appl. Opt.*, vol. 37, no. 36, pp. 8460–8476, 1998.

[27] K. Scholle, S. Lamrini, P. Koopmann, and P. Fuhrberg, "2 μm laser sources and their possible applications," *Front. Guided Wave Opt. Optoelectron.*, 2010.

[28] J. Wang, R. Xu, and S. Yang, "Estimation of plant water content by spectral absorption features centered at 1,450 nm and 1,940 nm regions," *Environ. Monit. Assess.*, vol. 157, pp. 459–469, 2009.

[29] K. Vizbaras *et al.*, "High power continuous-wave GaSb-based superluminescent diodes as gain chips for widely tunable laser spectroscopy in the 1.95-2.45 μm wavelength range," *Appl. Phys. Lett.*, vol. 107, 2015, Art. no. 011103.

[30] L. Shterengas *et al.*, "High-power 2.3-μm GaSb-based linear laser array," *IEEE Photon. Technol. Lett.*, vol. 16, no. 10, pp. 2218–2220, Oct. 2014.

[31] X. Li *et al.*, "High temperature characteristics of a 2 μm InGaSb/AlGaAsSb passively mode-locked quantum well laser," *Appl. Phys. Lett.*, vol. 114, 2019, Art. no. 221104.

[32] X. Li *et al.*, "Temperature- and current-dependent spontaneous emission study on 2 μm InGaSb/AlGaAsSb quantum well lasers," *Jpn. J. Appl. Phys.*, vol. 56, 2017, Art. no. 050310.